Double-template fabrication of three-dimensional porous nickel electrodes for hydrogen evolution reaction

I. Herraiz-Cardona[a], E. Ortega[a], L. Vázquez-Gómez[b], V. Pérez-Herranz[a,*]

[a] Ingeniería Electroquímica y Corrosión (IEC). Departamento de Ingeniería Química y Nuclear. Universitat Politècnica de València. Camino de Vera s/n. 46022 Valencia, Spain.

[b] IENI CNR, Corso Stati Uniti 4, 35127 Padova, Italy.

*Corresponding author. Tel.: +34-96-3877632; fax: +34-96-3877639;

E-mail address: vperez@iqn.upv.es (V. Pérez-Herranz)

Abstract

Three-dimensional (3D) porous nickel structures were fabricated via a double-template electrochemical deposition process. The construction of the foam structures was achieved by means of a hydrogen bubble dynamic template, prepared from Cu electrodeposition at high current densities. Subsequently, a Ni layer was electrodeposited on the Cu 3D template. During the nickel coating, the typical finger-like microstructure of the Cu foam becomes denser and changes to a cauliflower microstructure. The hydrogen evolution reaction (HER) on these macroporous Ni electrodes was evaluated in 30 wt.% KOH solution by means of polarization curves and electrochemical impedance spectroscopy (EIS). Results demonstrate greater apparent activity of the developed electrodes towards HER in comparison with commercial smooth Ni electrode. The 3D porous Ni electrocatalyst obtained from Cu templates synthesized at the lowest current density and the highest electrodeposition time yielded the best electrochemical activity for HER.

Keywords: 3D Ni Electrodeposits, Dynamic Template, Surface Roughness Factor, Electrochemical Impedance Spectroscopy.

1. Introduction

Hydrogen is considered an ideal energy carrier that can be an alternative to fossil fuels. It is a clean and fully recyclable substance with a practically unlimited supply, and has all the criteria considered for an alternative energy source. The electrochemical production of hydrogen by alkaline water electrolysis is one of the most promising methods with great potential of using renewable energy sources. Moreover, it represents an environmentally friendly technology for production of high purity hydrogen [1-5]. However, the high energy consumption of alkaline water electrolysers retrains its large-scale application at present. Although platinum shows the highest activity for the hydrogen evolution reaction (HER), new electrode materials have been investigated, aiming at the reduction of the cost associated with the electrocatalyst development. Among these materials, nickel and its alloys show a high initial electrocatalytic activity toward the HER [6-26]. The electrode activity can be enlarged by increasing the real surface area and/or the intrinsic activity of the electrode material [6].

One of the common ways to enlarge the real surface area is the utilization of Raney-type alloys from which the active component (Al, Zn) is dissolved by alkaline leaching. Caustic leaching of the alloy is accompanied by volume losses leading to pore and crack formation, yielding a highly porous catalytic nickel surface suitable for use in alkaline water electrolysis. Various techniques have been developed for the preparation of this type of electrodes, consisting in electrocodeposition of Raney-nickel powder with nickel [7–11], powder pressing of Raney-nickel [12–14], electrodeposition of Ni–Zn alloys [15–18] and thermal spraying of wires or powders [19–22].

Marozzi and Chialvo [23] developed pure Ni electrodeposits with macropores by galvanic deposition at very high apparent current densities of electrodeposition (up to 5 A cm^{-2}) from electrolytic solutions of $NiCl_2$ and NH_4Cl.

Porous materials prepared from template synthesis approaches have attracted considerably attention recently for their prospects in fabricating devices for magnetic, electronic, and electrochemical applications. Based on this technology, different high surface area Ni catalysts for HER have been successfully fabricated by means of electrodeposition on templates with proper porosities and layer/thickness, made of liquid crystal [24], polystyrene [25], or alumina [26].

This work describes a double-template synthesis of 3D porous Ni electrodes for HER. These electrodes were synthesized by nickel electrodeposition on copper foams obtained from hydrogen bubbles dynamic templates. The electrocatalytic performance of the developed electrodes for HER was evaluated in 30 wt.% KOH solution by using polarization curves and electrochemical impedance spectroscopy (EIS) techniques.

2. Experimental

2.1 Preparation of electrodes

The metallic coatings were deposited on an AISI 304 stainless steel substrate, embedded in Teflon, leaving a cross-sectional available area of 0.5 cm^2. AISI 304 stainless steel as substrate material was mainly chosen due to its good mechanical and corrosion resistance at relatively low cost.

Before the electrodeposition experiments, the stainless steel substrate was mechanically polished with emery paper down to 4000 grit, next it was degreased for 1 min with 25 wt.% NaOH at 90 ºC, immersed in HCl 18 wt.% during 1 min and anodically treated in 70 wt.% H_2SO_4 at 1080 A m^{-2} for 3 min. Then, the substrate surface was struck at 268 A m^{-2} in a Wood's nickel solution (240 g L^{-1} $NiCl_2$, 120 mL L^{-1} HCl) for 5 min, in order to produce a thin, adherent deposit of nickel which serves as a base for the subsequent electrodeposition. Between each treatment the electrode was rinsed with distilled water. The formation of electroactive coatings on such prepared AISI 304 stainless steel substrate was done by electrodeposition, following the schema shown in Fig.1. First of all, it was constructed a 3D porous copper structure by means of electrodeposition at high current densities in an acidic bath (0.05 M $CuSO_4$, 0.5 M H_2SO_4), and at room temperature. Since the hydrogen over-voltage of the substrate is low to generate hydrogen gas in highly acidic media and at high cathodic current densities, a large number of hydrogen bubbles created on the substrate move towards the electrolyte/air interface during the Cu electrodeposition process. Thus, the metal growth towards the gas bubble is prohibited simply because there are no metal ions available there, leading the electrodeposition between the gas bubbles (Fig. 1.a). In other words, the hydrogen bubbles function as a dynamic template during Cu deposition. Afterwards, the Cu macroporous layer acted as a template for the

nickel deposition (Fig. 1.b). Nickel, electrodeposited from a modified Watts bath (1.26 M $NiSO_4$, 0.19 M $NiCl_2$, 0.60 M H_3BO_3) at 50ºC, forms a continuous layer on the copper opal. The bath composition and deposition conditions of the tested electrodes are listed in Table 1. The structures, morphologies and compositions of the developed materials were examined by means of a JEOL JSM-3600 scanning electron microscope (SEM) coupled with an Energy Dispersive X-Ray (EDX) Spectrometer, and an OLYMPUS LEXT OLS3100-USS confocal laser scanning microscope.

Electrodepositions were carried out in a one-compartment cell made of Pyrex glass with a Teflon cover having adequate holes to lodge the electrodes. The solution inside the cell had an initial volume of 50 mL. The substrate surface was placed in horizontal position, allowing the free release of the produced hydrogen bubbles. The counter electrode was a large-area platinum electrode. The reference electrode was a commercially available silver-silver chloride (Ag-AgCl) electrode with 3 M KCl solution. The experiments were accomplished by using an AUTOLAB PGSTAT302N potentiostat/galvanostat.

2.2 Electrochemical measurements

The developed electrodes were characterized by means of polarization curves and electrochemical impedance spectroscopy (EIS). All these tests were performed in oxygen free 30 wt.% KOH solutions which were achieved by bubbling N_2 for 15 min before the experiments.

Polarization curves were potentiodynamically recorded from -1.60 V vs Ag/AgCl (-1.40 V vs SHE) up to the equilibrium potential at a scan rate of 1 mV s^{-1}, and at six different temperatures: 30, 40, 50, 60, 70 and 80 ºC. Before the tests, the working electrode was held at -1.60 V (vs Ag/AgCl) in the same solution in order to

reduce the oxide film existing on the surface electrode layer, for the time needed to establish reproducible polarization diagrams.

EIS measurements were performed after obtaining the polarization curves. Alternating current impedance measurements were carried out at different cathodic overpotentials, and at the following temperatures: 30, 50, and 80 ºC. The measurements were made in the frequency range of 10 kHz to 3 mHz. Ten frequencies per decade were scanned using a sinusoidal signal of 10 mV peak-to-peak. The complex nonlinear least square (CNLS) fitting of the impedance data was carried out with the Zview 3.0 software package.

The electrochemical measurements were carried out in an electrochemical cell developed by the Dpto. Ingeniería Química y Nuclear of the Universitat Politècnica de València [27]. It is a three-electrode cell with a heating circuit to control the temperature. A Luggin capillary, whose tip was set at a distance of about 1 mm from the surface of the working electrodes, was used to minimize the variations due to *jR*-drop in the electrolyte. In this system, the developed electrodes were used as the working electrodes, a large-area platinum electrode was employed as counter electrode, and the reference electrode was the same as that used in the electrodepositon process. The electrochemical experiments were performed using an AUTOLAB PGSTAT302N potentiostat/galvanostat.

3. Results and discussion

Fig. 2 shows the confocal laser scanning microscopy images of the porous 3D Cu-Ni layers synthesized following the electrochemical deposition conditions reported in both Table 1 and Fig. 1. The deposited films are characterized by a 3D foam structure. The origin of this unique structure is as discussed elsewhere [28] and briefly summarized in the experimental section. The resulting 3D copper structures are used as templates for generating 3D porous nickel films (Fig. 1.b). The galvanic replacement technique has not been used to generate the 3D nickel structure, due to the fact that copper is listed below nickel in the activity series, and no reaction occurs. The obtained copper foams are very weak, and collapse easily loosing the macroporous structure. The subsequent nickel electrodeposition considerably reinforces the copper electrodeposits, maintaining the opened foam layer. As depicted in Fig. 2, the macropore size of the foam increases with both the time of deposition and the decrease in the applied current density, i.e. the pore sizes of the material created by the hydrogen dynamic template increase with the distance away from the substrate, which is attributed to the coalescence of the hydrogen bubbles generated during the electrodeposition (see Fig. 1.a). Fig. 2.e shows a micrograph of the cross-section of the ED-2 electrode. The average coating thickness of the Cu/Ni layers, determined from the digital analysis of the confocal laser scanning images, is 265 ± 18 μm. The walls of the copper structure obtained by this method (before the nickel electrodeposition) are composed of numerous ramified deposits which constitute some nanoparticles (~300 nm), finger-like structure, similar to those previously reported in literature [28,29]. Moreover, there are many apertures away these branches to shape a loose porous structure, possibly due to local turbulences of electrolyte around the newly generated copper branches during deposition, as a consequence of a vigorous H_2 evolution [28,29]. Fig. 3 shows how the

microstructure of the Cu templates is modified with the subsequent Ni electrodeposition. Starting from the Cu template obtained at a current density of 0.5 A cm^{-2} during 360 s, as depicted in Fig. 3, as the time of the subsequent Ni electrodeposition increases, the microstructure of the coatings changes from the finger-like (Fig. 3.a) to the cauliflower structure (Fig. 3.b and 3.c). That is, nickel fills the gaps of the foam walls, making the ramified nanostructure much denser. It is important to control the nickel electrodeposition conditions, due to the fact that a thicker nickel layer blocks the macroporous structure, as it is observed in Fig. 2 for the ED-1 electrocatalyst. In order to ensure a complete nickel coating of the copper opal, nickel electrodeposition was carried out at least during 30 min at the conditions reported in Table 1. As derived from the chemical composition analysis, all the developed electrocatalysts shown in Fig. 2 present a superficial continuous nickel layer.

The catalytic activity of the prepared layer was evaluated by means of Tafel linear polarization measurements in 30 wt.% KOH solution. Fig. 4 shows a set of Tafel curves recorded at 50 ºC on the catalyst coatings investigated. A curve performed on commercial smooth Ni electrode was also included to compare the obtained results. Overpotentials were obtained from the recorded steady-state polarization curves by subtracting the reversible HER potential at the given conditions (i.e. -1.14 ± 0.01 V vs Ag/AgCl) and for the *jR*-drop. The information obtained from the Tafel polarization data demonstrate that all the investigated catalysts are very active for the HER, showing a higher catalytic activity than the smooth Ni electrode. Between all the tested 3D nickel electrocatalysts, ED-1 has the lowest catalytic activity for HER, which is attributed to a more intense nickel electrodeposition (1 hour) that considerably fills the macropores, generating a smoother layer and, consequently, a decrease in the active surface area. On the other hand, between ED-2 and ED-3 electrocatalysts it can be appreciated two

different regions: at overpotentials less cathodic than -150 mV, ED-3 electrode manifests a better catalytic activity than ED-2 coating, whereas this trend is inverted at more cathodic potentials. The reported behaviour is directly connected with the superficial morphology. The macropores of ED-3 electrocatalyst are blocked by gas bubbles when HER is vigorous, due to their smaller size, leading to low utilization of the whole surface. In contrast, the higher pore size of ED-2 catalyst facilitates the fast transport of electroactive gas through the porous electrode, increasing the hydrogen production for a same applied overpotential. Therefore, from Fig. 4 it is clear that the higher pore size of the catalyst surface the higher electrode activity, being ED-4 the best overall catalyst. The Tafel curves obtained for all the developed catalysts (Fig. 4) show a typical Tafelian behaviour, indicating that the HER on these electrodes is a purely kinetically controlled reaction described by the Tafel equation [30- 32]:

$$\eta = a + b \log j \tag{1}$$

where η (V) represents the applied overpotential, j (A cm^{-2}) the resulting (measured) current density, b (V decade^{-1}) the Tafel slope, and a (V) is the intercept related to the exchange current density j_0 (A cm^{-2}) through equation:

$$a = (2.3RT)/(\beta n_e F) \times \log j_0. \tag{2}$$

and n_e represents the number of electrons exchanged, F (=96,485 C mol^{-1}) is the Faraday constant, and R (= 8.314 J mol^{-1} K^{-1}) is the gas constant.

The values of the kinetic parameters determined from the polarization curves are reported in Table 2. The commonly accepted mechanism of hydrogen evolution consists of the following steps: (3) primary discharge step to produce adsorbed hydrogen (Volmer reaction) followed by either (4) electrochemical desorption (Heyrovsky reaction), or (5) chemical recombination (Tafel reaction)

$$H_2O + M + e^- \rightarrow MH_{ads} + OH^- \quad (3)$$

$$H_2O + MH_{ads} + e^- \rightarrow H_2 + M + OH^- \quad (4)$$

$$MH_{ads} + MH_{ads} \rightarrow H_2 + 2M \quad (5)$$

where M is a free site on the metal surface and MH_{ads} is the metal surface occupied by hydrogen adatoms. Assuming Volmer-Heyrovsky mechanism for the HER [33,34] according to equations (3)-(4) the linear part of Tafel curve at 30 ºC should yield a slope ca. 120 mV dec^{-1} when Volmer reaction is the rate determining step (*rds*) (140 mV dec^{-1} at 80 ºC) or 40 mV dec^{-1} for Heyrovsky reaction as the *rds* (47 mV dec^{-1} at 80 ºC) [33,34]. However, it has been shown that formally it is impossible to distinguish at which overpotential the *rds* changes when the slope is ca. 120 mV dec^{-1}, due to the fact that this Tafel slope value is also obtained when the surface coverage by adsorbed hydrogen, θ, tends to 1 and the *rds* is Heyrovsky [34]. When the Tafel slope is 30 mV dec^{-1} (35 mV dec^{-1} at 80 ºC) the *rds* is the Tafel reaction (5).

As it is shown in Table 2, Tafel slopes, b, obtained for all the coatings show that the HER proceeds via the same Volmer-Heyrovsky mechanism [34], ranging from 80 to 120 mV dec^{-1}, at 30 and 80 ºC, respectively. In contrast to the behaviour reported for the developed electrodes, the polarization curves recorded on the smooth Ni electrode (Fig. 2) display two potential-dependent regions related to the HER. The slope decreases from higher values at overpotentials less cathodic than approximately - 200 mV to lower values at more cathodic overpotentials. The existence of two Tafel regions has already been reported in literature on Ni-based catalysts [32-36]. At low cathodic overpotentials the Tafel slopes are higher than 120 mV dec^{-1} at 30 ºC.

It is evident that the influence of temperature on the values in Table 2 is significant. The exchange current densities, j_0, of the developed electrocatalysts increase with temperature, which is the expected kinetic behaviour. Moreover, as depicted in

Table 2, exchange current density values of the smooth Ni electrode at different temperatures are in the range of 0.01 and 10 μA cm^{-2}, whereas for the developed coatings range between 0.01 and 10 mA cm^{-2}, which indicates a considerable improvement of the apparent electrocatalytic properties of the fabricated electrodes.

In order to better compare the electrocatalytic activity of the catalysts from the polarization curves, one can fix a current density value and compare the resulting overpotentials required to reach the given current density. This would give an indication on the amount of energy (overpotential) that has to be invested to produce a fixed amount of hydrogen, since the current is directly related to the amount of produced hydrogen through the Faraday's law. Fig. 5 shows the overpotential values of the synthesized electrocatalysts at a fixed current density of 100 mA cm^{-2}, η_{100}, in 30 wt.% KOH solution at different temperatures. As expected, the values decrease with increasing temperature, indicating that the catalysis property is improved with the increase in temperature. From Fig. 5 it is easily shown the better catalytic behaviour of the developed catalysts with respect to the smooth Ni electrode, manifesting a reduction in the energy requirements that ranges between 25 and 70%. As derived from both Table 2 and Fig. 5, the highest exchange current density and the lowest η_{100} values are obtained for the ED-4 cathode, indicating that this electrode is the best overall catalyst. The η_{100} values obtained for the ED-4 electrode reveal an electrochemical activity higher and/or in the same order of magnitude than that previously reported by other authors for Raney-Ni, NiMo, NiLa, Ni/MoS_2, NiP, etc. [6].

To ensure a complete characterization of the electrode/electrolyte interface and corresponding processes, EIS measurements were made at different selected overpotentials of the previously obtained polarization curves. Figure 6 show examples of EIS spectra recorded on the ED-2, and ED-4 electrocatalysts. The Nyquist

representation of the impedance data recorded on the ED-2 coating (Fig. 6.a.1) reveals the presence of two strongly overlapped semicircles (i.e. two different time constants). This behaviour was also observed for both ED-1 and ED-3 electrodes. With respect to the impedance spectra of the ED-4 electrode, it is shown that the two semicircles in the Nyquist plot are clearly differentiated (Fig. 6.b.1), and two maximums appear in the Bode representation of the phase angle as a function of frequency (Fig. 6.b.2). In all the cases, at the higher cathodic overpotential applied, HER is so vigorous that hydrogen bubbles cause too much interference, good impedance spectra cannot be obtained and only one deformed semicircle appears. Similar behaviour has been reported by Choquette et al. [9,10] and Okido et al.[37]. From Fig. 6.a.1 and 6.b.1 it is clear that the diameter of both semicircles in the Nyquist plots considerably diminishes with the cathodic overpotential for all the investigated electrodes. The same phenomenon was evidenced with the increase in the temperature, indicating that both time constants are related to the electrode kinetics [21].

To model the experimental data of the impedance response characterized by one semicircle in the Nyquist plot (i.e. recorded at highest overpotentials) it has been used the one time constant (1T) electric equivalent circuit (EEC) model. This model is the classical Randles EEC in which the double layer capacitance was replaced by a constant phase angle element (CPE), see Fig. 7.a [14,15]. CPE is defined in impedance representation as:

$$Z_{CPE} = \left[Q \cdot (i \cdot \omega)^{n}\right]^{-1} \tag{6}$$

where Q is the CPE constant, ω is the angular frequency (in rad/s), i^2 = -1 is the imaginary number, and n is the CPE exponent.

With respect to the impedance response characterized by two semicircles in the Nyquist plot, according to the behaviour of the high frequency semicircle with both

overpotential and temperature, and following the criteria previously used in refs.[21,31,33,38,39], in order to derive a physical picture of the electrode/electrolyte interface and the processes occurring at the electrode surface, the two-time constant parallel (2TP) EEC model (see Fig. 7.b) has been used to fit the EIS response of the catalysts investigated. The 2TP model (Fig. 7.b) represents a slightly modified model, originally proposed by Armstrong and Henderson [40], in which the double layer capacitance was replaced by a CPE [21,34]. The 2TP model reflects the response of a HER system characterized by two semicircles (i.e. two time constants): the high frequency (HF) semicircle, τ_1 (CPE_1, R_1), related to the charge transfer kinetics, and the low frequency (LF) semicircle, τ_2 (CPE_2, R_2), related to the hydrogen adsorption [21,31,33,38,39].

Fig. 6 shows that a very good agreement between the experimental (symbols) and CNLS approximations (lines) data is obtained when these models are used to describe the EIS response of the developed catalysts. Table 3 shows the best-fit estimates of the different EEC parameters obtained from the impedance measurements of both ED-2 and ED-4 electrodes at different overpotentials and temperatures. The average double layer capacitances, C_i, for the catalytic coatings were determined using the relation suggested by Brug et al. [41]:

$$C_i = [Q_i / (R_S^{-1} + R_i^{-1})^{(1-n_i)}]^{1/n_i} \quad (7)$$

According to the EEC parameter values presented in Table 3, the two time constants, τ_1 (CPE_1, R_1) and τ_2 (CPE_2, R_2), decrease with the cathodic overpotential and the temperature, indicating that both semicircles are related to the kinetics of the process [21]. Both the C_1 and the R_1 decrease with cathodic overpotential for all the developed electrocatalysts. Hence, the first time constant, τ_1 or HF time constant, is related to the HER charge-transfer kinetics, namely to the response of double layer capacitance

characterized by CPE_1, and HER charge transfer resistance characterized by R_1. On the other hand, it can be distinguished two different behaviours of the second time constant, τ_2 or LF time constant, for the tested electrodes. With an increase in the cathodic overpotential, the value of C_2 increases, while the value of R_2 decreases for the ED-4 cathode. This is a typical behaviour related to the response of hydrogen adsorbed on an electrode surface, namely to the hydrogen adsorption pseudocapacitance, CPE_2, and resistance R_2 [21,31,33,38,39]. In contrast, in the case of ED-1, ED-2, and ED-3 electrocatalysts, the C_2 and the R_2 rapidly decrease with overpotential. Current results do not allow us to make a definite conclusion on the physical behaviour of the LF time constant, but the overpotential trend of C_2, n_2, and R_2, and their absolute values indicate that the observed LF response could be related to a response of some fast transfer processes (most likely charge, rather than mass) in impurities (e.g. iron) deposited on the electrode surface, coming from trace contaminations present in even very pure alkaline solutions [6,42]. For all the electrodes, at more negative overpotential the semicircle related to the adsorption relaxation apparently completely disappears and only the semicircle related to the charge transfer remain observable. This is due to the fact that the adsorption process is facilitated and the charge-transfer process dominates the impedance response as the potential increases. Hence, HER is controlled by Heyrovsky step [42-44].

Besides the information on the kinetics of the HER, EIS results can be also used to estimate the real surface area of electrocatalytic coatings. This is important since by knowing the real electrochemically active area of the catalyst, it is possible to conclude on the intrinsic activity of the material in the HER, by subtracting for the surface area effect. Considering a value of 20 μF cm^{-2} for the double layer capacitance, C_{dl}, of a smooth nickel surface, used earlier in the literature [35,38], the real active surface area,

in terms of surface roughness factor (R_f), may be estimated by comparing the C_{dl} related to the HER charge-tranfer kinetics (C_1) of porous/rough and smooth electrodes [43]. The plots of the electrode R_f as function of the HER overpotential are displayed in Fig. 8. As it is clear from Fig. 8, the values of R_f decrease when increasing the cathodic potential. This indicates that a fraction of the inner surface of the electrode is blocked during HER due to gas bubbles shielding, and hence not electrochemically accessed by the electrolyte [22,24,46-48]. The R_f values obtained for the developed electrodes at all the investigated conditions are collected in Table 4. ED-1 electrocatalyst presents the lower R_f values, which is explained due to the pore filler caused by the thicker Ni coating. On the other hand, the higher R_f values are obtained for the ED-4 catalyst, as a consequence of a higher pore size (see Fig.2) that allows a better access of the electrolyte to the surface and an easier hydrogen bubble release from the electrode. From Fig. 8 it is also derived that, although the ED-3 electrode shows a higher percentage of pores than the ED-2 electrode (see Fig.2), those pores are not completely contributing to the electrochemical active surface area of the electrode. This phenomenon is also explained in terms of the pore size: the smaller pores are blocked by the generated hydrogen bubbles and, therefore, not accessed by the electrolyte. R_f values obtained for our best electrode (ED-4) are ca. 10^3, higher and/or comparable to those reported for porous nickel electrodes obtained by galvanic deposition at very high current densities [49], as well as those reported for Raney Ni-Zn electrodeposited [15], Raney Ni-Zn pressed powder electrodes [14], and thermal arc sprayed skeleton nickel electrodes [22]. The agreement between the EIS study and the polarization study let us conclude that the improvement in the catalytic activity of the developed electrodes is mainly attributed to increase in the active surface area.

4. Conclusions

Three-dimensional foam Ni structures were successfully created by a double-template electrochemical procedure: Ni was electrodeposited on a macroporous Cu opal, previously obtained from a hydrogen bubble dynamic template generated by electrochemical deposition processes. The typical finger-like microstructure of the Cu template pore walls is turned into a cauliflower microstructure, after the Ni coating. The hydrogen evolution reaction (HER) on these electrodes was assessed by polarization curves and electrochemical impedance spectroscopy (EIS). This research allowed us to enhance that:

1. The investigated catalysts manifest greater apparent activity towards HER in comparison with commercial smooth Ni electrode, obtaining for the best overall catalyst (ED-4) exchange current densities three magnitude orders higher than that reported for the commercial smooth Ni electrode.
2. An excessive Ni coating on the copper template diminishes the active surface area of the electrodes, decreasing the catalytic activity of the electrode.
3. Copper opals obtained at lower current densities and higher deposition times (ED-4) lead to 3D Ni catalysts with a higher pore size. The higher the pore sizes of the macroporous catalyst, the higher the electrode activity.
4. The HER on the developed electrocatalysts is controlled by the Volmer-Heyrovsky mechanism.
5. From both linear Tafel polarization curves and EIS it is derived that the increase in the catalytic activity of the developed electrodes is mainly attributed to an increase in the electrochemical active surface area.

Acknowledgements

Isaac Herraiz-Cardona is grateful to the Ministerio de Educación (Spain) for a postgraduate grant (Ref. AP2007-03737). This work was supported by Generalitat Valenciana (PROMETEO/2010/023) and Universidad Politécnica de Valencia (PAID-06-10-2227).

References

[1] Veziroglu TN, Barbir F. Hydrogen - the wonder fuel. Int J Hydrogen Energy 1992;17:391-404.

[2] Elosta WB, Veziroglu TN. Solar hydrogen energy system for a Libyan coastal county. Int J Hydrogen Energy 1990;15:33-44.

[3] Bockris JO, Veziroglu TN. A solar-hydrogen economy for USA. Int J Hydrogen Energy 1983;8:323-340.

[4] Hug W, Divisek J, Mergel J, Seeger W, Steeb H. Highly efficient advanced alkaline electrolyzer for solar operation. Int J Hydrogen Energy 1992;17:699-705.

[5] Garciaconde AG, Rosa F. Solar hydrogen-production - A Spanish experience. Int J Hydrogen Energy 1993;18:995-1000.

[6] Lasia A. Hydrogen Evolution. In: Vielstich W, Lamm A, Gasteiger HA, editors. Handbook of fuel cells-Fundamentals, Technology and Applications, John Wiley and Sons Ltd; 2003, p. 416-440.

[7] Endoh E, Otouma H, Morimoto T, Oda Y. New Raney nickel composite-coated electrode for hydrogen evolution. Int J Hydrogen Energy 1987;12:473-479.

[8] Choquette Y, Menard H, Brossard L. Hydrogen discharge on a Raney nickel composite-coated electrode. Int J Hydrogen Energy 1989;14:637-642.

[9] Choquette Y, Brossard L, Lasia A, Menard H. Investigation of hydrogen evolution on Raney-nickel composite-coated electrodes. Electrochim Acta 1991;35:1251-1256.

[10] Choquette Y, Brossard L, Lasia A, Menard H. Study of the kinetics of hydrogen evolution reaction on Raney Nickel composite-coated electrode by AC impedance technique. J Electrochem Soc 1990;137:1723-1730.

[11] Endoh E, Otouma H, Morimoto T. Advanced low hydrogen overvoltage cathode for chlor-alkali electrolysis cell. Int J Hydrogen Energy 1988;13:207-213.

[12] Los P, Rami A, Lasia A. Hydrogen evolution reaction on Ni-Al electrodes. J Appl Electrochem 1993;23:135-140.

[13] Hitz C, Lasia A. Experimental study and modeling of impedance of the her on porous Ni electrodes. J Electroanal Chem 2001;500:213.

[14] Chen L, Lasia A. Study of the Kinetics of Hydrogen Evolution Reaction on Nickel-Zinc Powder Electrodes. J Electrochem Soc 1992;139:3214.

[15] Chen L, Lasia A. Study of the kinetics of hydrogen evolution reaction on nickel–zinc alloy electrodes. J Electrochem Soc 1991;138:3321.

[16] Balej J, Divisek J, Schmitz H, Mergel J. Preparation and properties of raney nickel electrodes on Ni–Zn base for H_2 and O_2 evolution from alkaline solutions Part I: electrodeposition of Ni–Zn alloy from chloride solutions. J Appl Electrochem 1992;22:705.

[17] de Giz MJ, Machado SAS, Avaca LA, González ER. High area Ni–Zn and Ni–Co–Zn codeposits as hydrogen electrodes in alkaline solutions. J Appl Electrochem 1992;22:973.

[18] Sheela G, Pushpavanam M, Pushpavanam S. Zinc–nickel alloy electrodeposits for water electrolysis. Int J Hydrogen Energy 2002;27:627.

[19] Miousse D, Lasia A, Borck V. Hydrogen evolution reaction on Ni–Al–Mo and Ni–Al electrodes prepared by low pressure plasma spraying. J Appl Electrochem 1995;25:592.

[20] Fournier J, Miousse D, Legoux JG.Wire-arc sprayed nickel based coating for hydrogen evolution reaction in alkaline solutions. Int J Hydrogen Energy 1999;24:519.

[21] Birry L, Lasia A. Studies of the hydrogen evolution reaction on Raney–nickel–molybdenum electrodes. J Appl Electrochem 2004;34:735.

[22] Kellenberger A, Vaszilcsin N, Brandl W. Roughness factor evaluation of thermal arc sprayed skeleton nickel electrodes. J Solid State Electr 2007;11:84.

[23] Marozzi CA, Chialvo AC. Development of electrode morphologies of interest in electrocatalysis. Part 1: Electrodeposited porous nickel electrodes. Electrochim Acta 2000;45:2111-2120.

[24] Ganesh V, Lakshminarayanan V. Preparation of high surface area nickel electrodeposit using a liquid crystal template technique. Electrochim Acta 2004;49:3561-3572.

[25] Huang YJ, Lai CH, Wu PW, Chen LY. Ni inverse opals for water electrolysis in an alkaline electrolyte. J Electrochem Soc 2010;157:18-22.

[26] Lee K, Yi Y, Lee HJ, Uhm S, Lee J. Electrocatalytic activity of Ni nanowires prepared by galvanic electrodeposition for hydrogen evolution reaction. Catal Today 2009;146:188-191.

[27] García-Antón J, Blasco-Tamarit E, García-García DM, Guiñón-Pina V, Leiva-García R, Pérez-Herranz V. 2008: P200803389.

[28] Shin HC, Dong J, Liu M. Nanoporous structures prepared by an electrochemical deposition process. Adv Mater 2003;15:1610-1614.

[29] Shin HC, Liu M. Copper foam structures with highly porous nanostructured walls. Chem Mater 2004;16:5460-5464.

[30] Southampton Electrochemistry Group, Instrumental methods in electrochemistry, Wiley, New York (1985).

[31] Herraiz-Cardona I, Ortega E, García Antón J, Pérez-Herranz V. Assessment of the roughness factor effect and the intrinsic catalytic activity for hydrogen evolution reaction on Ni-based electrodeposits. Int J Hydrogen Energy 2011;36: 9428-9438.

[32] Domínguez-Crespo MA, Torres-Huerta AM, Brachetti-Sibajab B, Flores-Vela A. Electrochemical performance of Ni–RE (RE = rare earth) as electrode material for hydrogen evolution reaction in alkaline medium. Int J Hydrogen Energy 2011;36:135–151.

[33] Navarro-Flores E, Chong ZW, Omanovic S. Characterization of Ni, NiMo, NiW and NiFe electroactive coatings as electrocatalysts for hydrogen evolution in an acidic medium. J Mol Cat A: Chemical 2005;226:179-197.

[34] Lasia A, Rami A. Kinetics of hydrogen evolution on Nickel electrodes. J Electroanal Chem 1990;294:123-141.

[35] Rami A, Lasia A. Kinetics of hydrogen evolution on Ni-Al Alloy electrodes. J Appl Electrochem 1992;22:376-382.

[36] Metikos-Hukovic A, Grubac Z, Radic N, Tonejc A. Sputter deposited nanocrystalline Ni and Ni-W films as catalysts for hydrogen evolution. J Mol Cat A: Chemical 2006;249:172-180.

[37] Okido M, Depo JK, Capuano GA. The mechanism of hydrogen evolution reaction on a modified Raney-Nickel composite-coated electrode by AC impedance. J Electrochem Soc 1993;140:127-133.

[38] Herraiz-Cardona I, Ortega E, Pérez-Herranz V. Impedance study of hydrogen evolution on Ni/Zn and Ni-Co/Zn stainless steel based electrodeposits. Electrochim Acta 2011;56:1308-1315.

[39] Simpraga R, Tremiliosi-Filho G, Qian SY, Conway BE. In situ determination of the ‘real area factor' in H_2 evolution electrocatalysis at porous Ni---Fe composite electrodes. J Electroanal Chem 1997;424:141-151.

[40] Armstrong RD, Henderson M. Impedance plane display of a reaction with an adsorbed intermediate. J Electroanal Chem 1972;39:81-90.

[41] Brug GJ, Vandeneeden ALG, Sluytersrehbach M, Sluyters JH. The analysis of electrode impedances complicated by the presence of a constant phase element. J Electroanal Chem 1984;176:275-295.

[42] Bai L, Harrington DA, Conway BE. Behavior of overpotential-deposited species in faradic reactions-II. AC impedance measurements on H_2 evolution kinetics at activated and unactivated Pt cathodes, Electrochim Acta 1987;32:1713-1731.

[43] Harrington DA, Conway BE. AC impedance of faradic reactions involving electrosorbed intermediates-I. Kinetic Theory, Electrochim Acta 1987;32:1703-1712.

[44] Lasia A. Impedance of porous electrodes. In: Conway BE, White RE, editors. Modern aspects of electrochemistry, Kluwer Academy/Plenum Publishers; 2002; vol. 35, p. 1-49.

[45] Trasatti S. Electrocatalysis: understanding the success of DSA. Electrochim Acta 2000;45:2377-2385.

[46] Kellenberger A, Vaszilcsin N, Brandl W, Duteanu N. Kinetics of hydrogen evolution reaction on skeleton nickel and nickel-titanium electrodes obtained by thermal arc spraying technique. Int J Hydrogen Energy 2007;32:3258-3265.

[47] Rausch S, Wendt H. Morphology and Utilization of Smooth Hydrogen-Evolving Raney Nickel Cathode Coatings and Porous Sintered-Nickel Cathodes. J Electrochem Soc 1996;143:2852-2862

[48] Pierozynski B, Smoczynski L. Kinetics of hydrogen evolution reaction at Nickel-Coated carbon fiber materials in 0.5 M H_2SO_4 and 0.1 M NaOH solutions. J Electrochem Soc 2009;156:B1045-B1050.

[49] Huet F, Musiani M, Nogueira RP. Oxygen evolution on electrodes of different roughness: an electrochemical noise study. J Solid State Electrochem 2004;8:786-793.

LIST OF TABLES

LIST OF FIGURES

Figure 8. Surface roughness factor, R_f, as a function of the overpotential for the developed electrodes in 30 wt.% KOH solution at 50 ºC.

Table 1. Bath compositions and operating conditions used in the electrodeposition of electrocatalytic coatings on an AISI 304 stainless steel substrate.

Catalyst	Cu Template formation		Ni Electrodeposition	
	Bath Composition / M		Bath Composition / M	
	$CuSO_4$ H_2SO_4	0.05 0.50	$NiSO_4$ $NiCl_2$ H_3BO_3	1.26 0.19 0.60
	i / A cm^{-2}	Time / s	i / A cm^{-2}	Time / s
ED-1	0.5	360	0.05	3600
ED-2	0.5	360	0.05	1800
ED-3	1.0	180	0.05	1800
ED-4	0.2	450	0.05	1800

Table 2. Kinetic parameters of the HER obtained from the polarization curves recorded in 30 wt.% KOH solution at different temperatures.

Catalyst		Temperature (ºC)					
		30	40	50	60	70	80
Smooth Ni							
	$b_{l\eta}$ **(mV dec^{-1})**	255.7	235.6	240.3	223.6	256.3	249.8
	$b_{h\eta}$ **(mV dec^{-1})**	97.9	103.7	107.5	122.8	137.3	171.4
	i_0 **(μA cm^{-2})**	0.07	0.16	0.44	0.92	2.00	4.77
ED-1							
	b **(mV dec^{-1})**	90.5	103.8	108.1	108.2	108.3	111.6
	i_0 **(mA cm^{-2})**	0.01	0.04	0.05	0.08	0.14	0.18
ED-2							
	b **(mV dec^{-1})**	83.8	88.0	92.4	101.7	114.8	123.2
	i_0 **(mA cm^{-2})**	0.04	0.08	0.08	0.10	0.22	0.39
ED-3							
	b **(mV dec^{-1})**	87.3	102.9	108.6	126.9	130.9	136
	i_0 **(mA cm^{-2})**	0.05	0.15	0.15	0.29	0.36	0.49
ED-4							
	b **(mV dec^{-1})**	102.5	105.0	108.9	110.5	112.3	115.9
	i_0 **(mA cm^{-2})**	2.64	3.76	4.37	4.89	6.86	8.50

Table 3. EEC parameters obtained by fitting EIS experimental spectra recorded at various overpotentials and temperatures in 30 wt.% KOH solution on the investigated electrocatalytic coatings.

Catalyst	Temperature / ºC							
	30				80			
ED-2								
η / mV	0	-35	-125	-220	0	-73	-170	-235
χ^2	$9.45\cdot10^{-4}$	$7.91\cdot10^{-4}$	$7.93\cdot10^{-4}$	$6.00\cdot10^{-4}$	$3.20\cdot10^{-4}$	$6.33\cdot10^{-4}$	$5.79\cdot10^{-4}$	$8.87\cdot10^{-4}$
R_S / Ω cm^2	0.56 ± 0.02	0.56 ± 0.02	0.57 ± 0.01	0.57 ±0.01	0.31 ± 0.01	0.31 ± 0.01	0.32 ± 0.02	0.33 ± 0.01
R_1 / Ω cm^2	278.9 ± 9.3	169.1 ± 7.4	21.2 ± 5.1	1.6 ± 0.5	24.2 ± 3.2	24.0 ± 1.2	7.6 ± 0.7	1.0 ± 0.1
R_2 / Ω cm^2	1506.0 ± 22.4	244.4 ± 8.3	-	-	616.0 ± 18.1	41.1 ± 5.4	-	-
Q_1 / mΩ^{-1} cm^{-2} s^n	5.67 ± 0.95	3.81 ± 0.62	2.55 ± 0.60	2.46 ± 0.33	7.85 ± 1.12	3.52 ± 0.87	2.69 ± 0.55	2.31 ± 0.30
n_1	0.95 ± 0.02	0.97 ± 0.01	0.97 ± 0.01	0.96 ± 0.02	0.92 ± 0.03	0.97 ± 0.01	0.97 ± 0.01	0.99 ± 0.01
C_1 / mF cm^{-2} *	4.20 ± 1.21	3.21 ± 0.72	2.15 ± 0.63	1.89 ± 0.34	4.56 ± 1.14	2.79 ± 0.88	2.11 ± 0.57	2.14 ± 0.32
Q_2 / mΩ^{-1} cm^{-2} s^n	9.91 ± 1.55	12.59 ± 2.17	-	-	46.0 ± 7.3	19.8 ± 1.7	-	-
n_2	0.57 ± 0.07	0.50 ± 0.06	-	-	0.51 ± 0.02	0.37 ± 0.05	-	-
C_2 / mF cm^{-2} *	19.0 ± 1.7	15.9 ± 2.0	-	-	49.6 ± 7.6	2.7 ± 1.8	-	-
τ_1 / s #	$1.2\cdot10^{0}$	$5.4\cdot10^{-1}$	$4.6\cdot10^{-2}$	$3.0\cdot10^{-3}$	$1.1\cdot10^{-1}$	$6.7\cdot10^{-2}$	$1.6\cdot10^{-2}$	$2.1\cdot10^{-3}$
τ_2 / s #	$28.6\cdot10^{0}$	$3.9\cdot10^{0}$	-	-	$30.6\cdot10^{0}$	$1.1\cdot10^{-1}$	-	-
ED-4								
η / mV	0	-30	-50	-105	0	-30	-50	-116
χ^2	$9.77\cdot10^{-4}$	$1.16\cdot10^{-3}$	$7.47\cdot10^{-4}$	$1.85\cdot10^{-3}$	$1.01\cdot10^{-3}$	$5.73\cdot10^{-4}$	$4.94\cdot10^{-4}$	$9.93\cdot10^{-4}$
R_S / Ω cm^2	0.61 ± 0.02	0.58 ± 0.02	0.57 ± 0.02	0.57 ± 0.02	0.34 ± 0.02	0.34 ± 0.01	0.33 ± 0.01	0.34 ± 0.01
R_1 / Ω cm^2	5.87 ± 0.85	4.11 ± 0.45	3.55 ± 0.31	1.36 ± 0.09	2.46 ± 0.25	4.40 ± 0.33	6.97 ± 1.13	3.20 ± 0.27
R_2 / Ω cm^2	147.1 ± 11.2	2.4 ± 0.5	1.3 ± 0.2	-	199.7 ± 31.4	10.9 ± 2.1	3.3 ± 0.9	-
Q_1 / mΩ^{-1} cm^{-2} s^n	30.4 ± 5.4	21.5 ± 4.3	18.5 ± 2.0	15.0 ± 1.5	23.2 ± 2.2	14.1 ± 1.8	11.4 ± 1.9	8.9 ± 1.5
n_1	0.93 ± 0.01	0.93 ± 0.01	0.93 ± 0.01	0.91 ± 0.02	0.91 ± 0.01	0.94 ± 0.02	0.93 ± 0.02	0.95 ± 0.01
C_1 / mF cm^{-2} *	22.6 ± 5.5	15.3 ± 4.3	12.7 ± 2.2	9.1 ± 1.5	14.5 ± 3.2	10.1 ± 2.2	7.6 ± 1.0	6.5 ± 1.1
Q_2 / Ω^{-1} cm^{-2} s^n	3.69 ± 1.10	7.19 ± 1.50	8.38 ± 1.51	-	2.60 ± 0.94	1.67 ± 0.49	3.86 ± 0.21	-
n_2	0.85 ± 0.03	0.89 ± 0.02	0.86 ± 0.02	-	0.86 ± 0.02	0.65 ± 0.01	0.96 ± 0.01	-
C_2 / F cm^{-2} *	6.29 ± 1.67	9.79 ± 1.84	11.71 ± 1.52	-	3.58 ± 1.20	4.13 ± 0.51	4.22 ± 0.31	-
τ_1 / s #	$1.3\cdot10^{-1}$	$6.3\cdot10^{-2}$	$4.5\cdot10^{-2}$	$1.2\cdot10^{-2}$	$3.6\cdot10^{-2}$	$4.4\cdot10^{-2}$	$5.3\cdot10^{-2}$	$2.1\cdot10^{-2}$
τ_2 / s #	$9.3\cdot10^{2}$	$2.3\cdot10^{1}$	$1.5\cdot10^{1}$	-	$7.1\cdot10^{2}$	$4.5\cdot10^{1}$	$1.4\cdot10^{1}$	-

* Calculated using Eq. (7)

Calculated from the best-fit estimates of EEC parameters.

Table 4. Surface roughness factors, R_f, determined from the EIS study on the investigated electrocatalytic coatings at 30 wt.% KOH solution.

Catalyst		Temperature / ºC											
		30				50				80			
ED-1	η / mV	0	- 205	- 301	-	0	- 72	- 151	- 247	0	- 154	- 242	-
	R_f	36	15	14	-	26	23	14	12	22	11	9	-
ED-2	η / mV	0	-35	-125	-220	0	- 54	- 151	- 236	0	-73	-170	-235
	R_f	210	161	107	94	239	163	120	108	228	139	106	107
ED-3	η / mV	0	- 145	- 232	-	0	- 45	- 131	- 226	0	162	252	-
	R_f	104	57	50	-	159	121	72	59	180	60	56	-
ED-4	η / mV	0	- 30	- 50	- 105	0	- 32	- 49	- 104	0	-30	-50	-116
	R_f	1128	764	636	457	1034	664	575	410	725	497	378	325

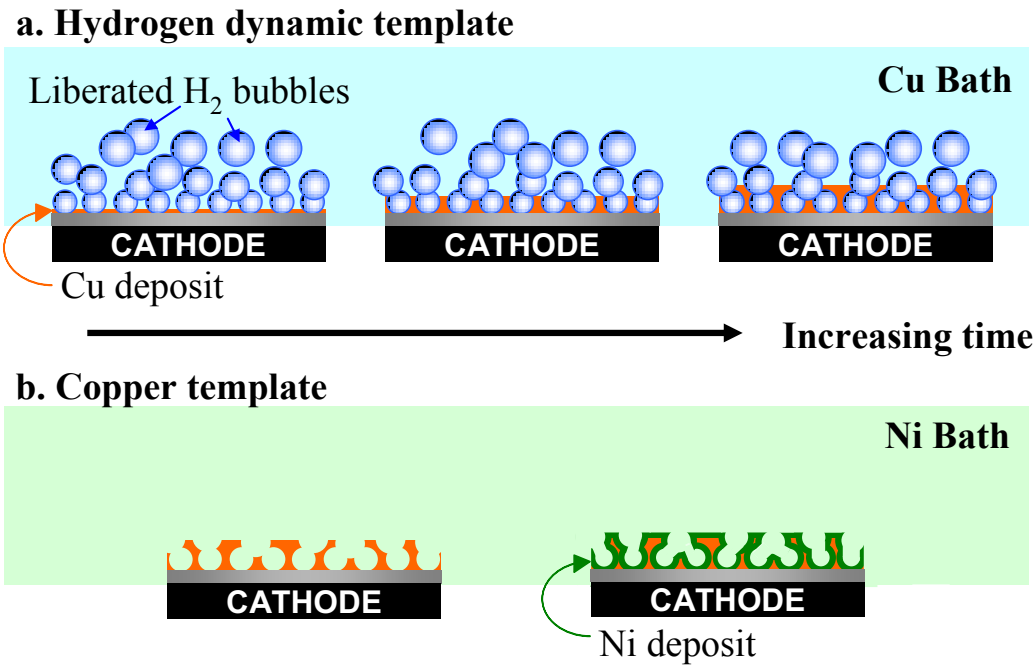

Figure 1. Simplified description of the formation process of the 3D macroporous electrodes. A serie of gas bubbles, evolved at different locations on the substrate, acts as a dynamic template during the course of copper growth (**a**). After the copper 3D deposit is obtained it is used as a template for the Ni electrodeposition (**b**).

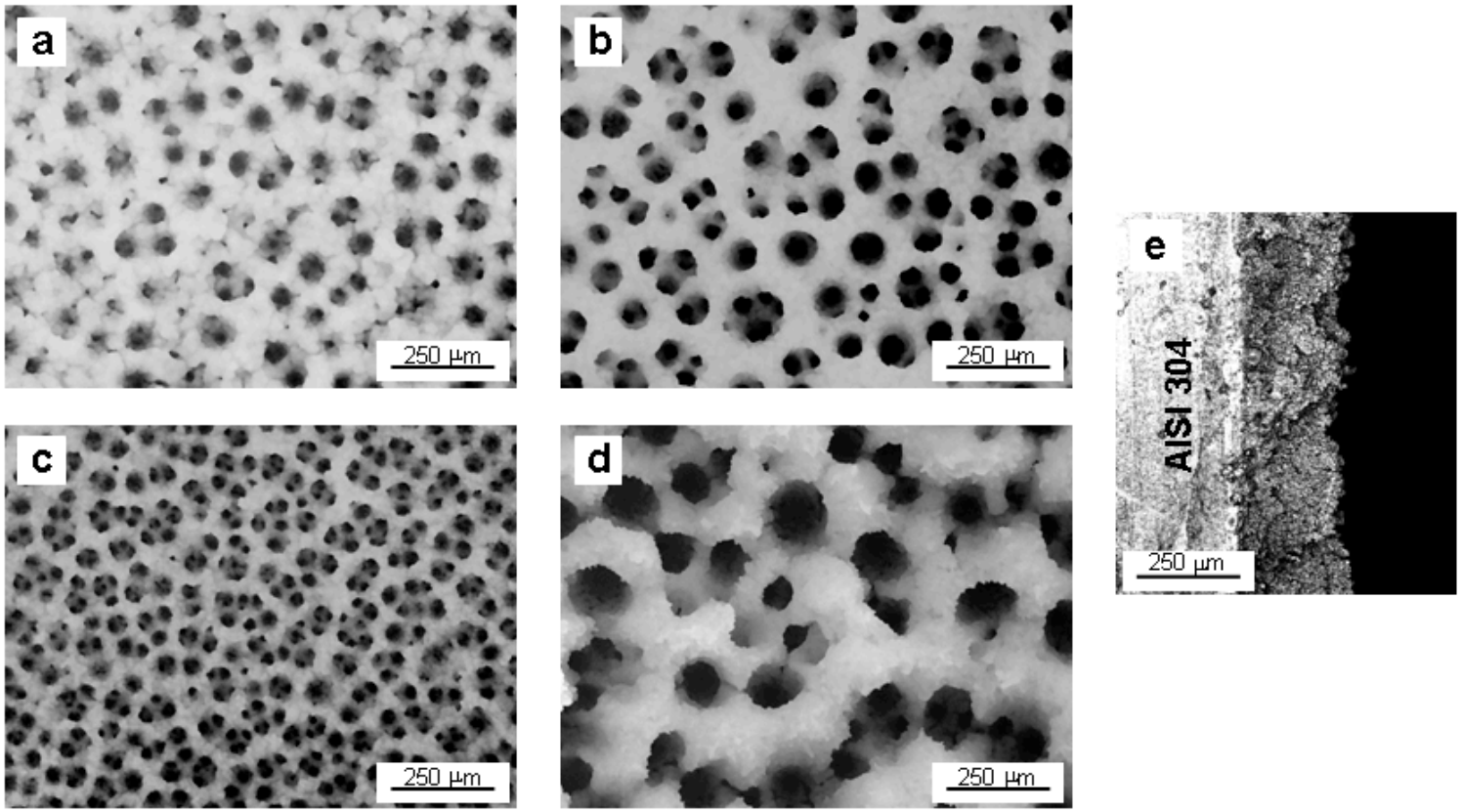

Figure 2. Confocal laser scanning micrographs of the 3D Cu structures after the Ni electrodeposition as-deposited: **a**. ED-1, **b**. ED-2, **c**. ED-3, **d**. ED-4 electrode, and **e**. Cross-section of the ED-2 electrode.

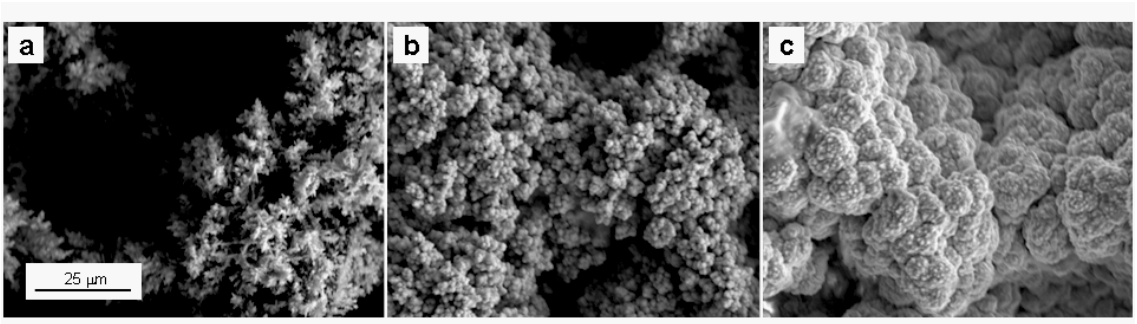

Figure 3. SEM images of the evolution of the electrode microstructure during the Ni coating on the Cu template obtained at 0.5 A cm^{-2} and 360 s, after different Ni electrodeposition times: **a**. 15 min; **b**. 30 min (ED-2 electrode); **c**. 60 min (ED-1 electrode).

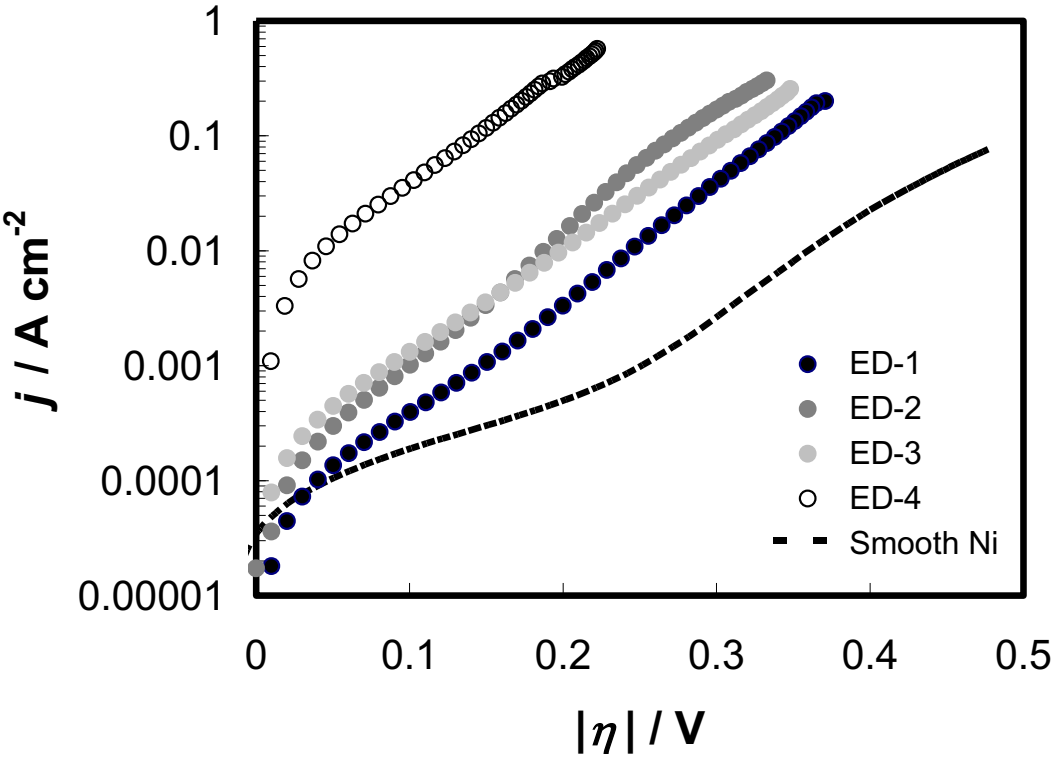

Figure 4. Linear Tafel polarization curves recorded on the different developed electrodes in 30 wt.% KOH solution at 50 ºC.

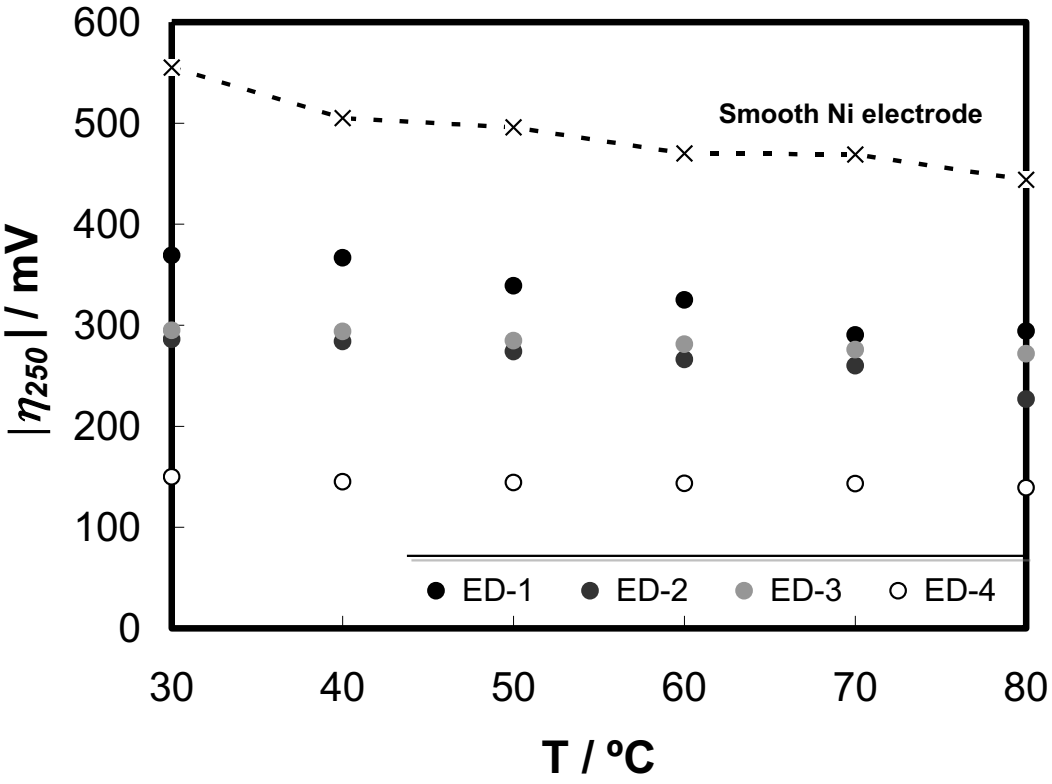

Figure 5. Comparison of the electrocatalytic activity of the developed electrocatalysts in terms of the overpotential needed for a fixed hydrogen production rate determined by the current density of -100 mA cm^{-2}, η_{100}, in 30 wt.% KOH at different temperatures.

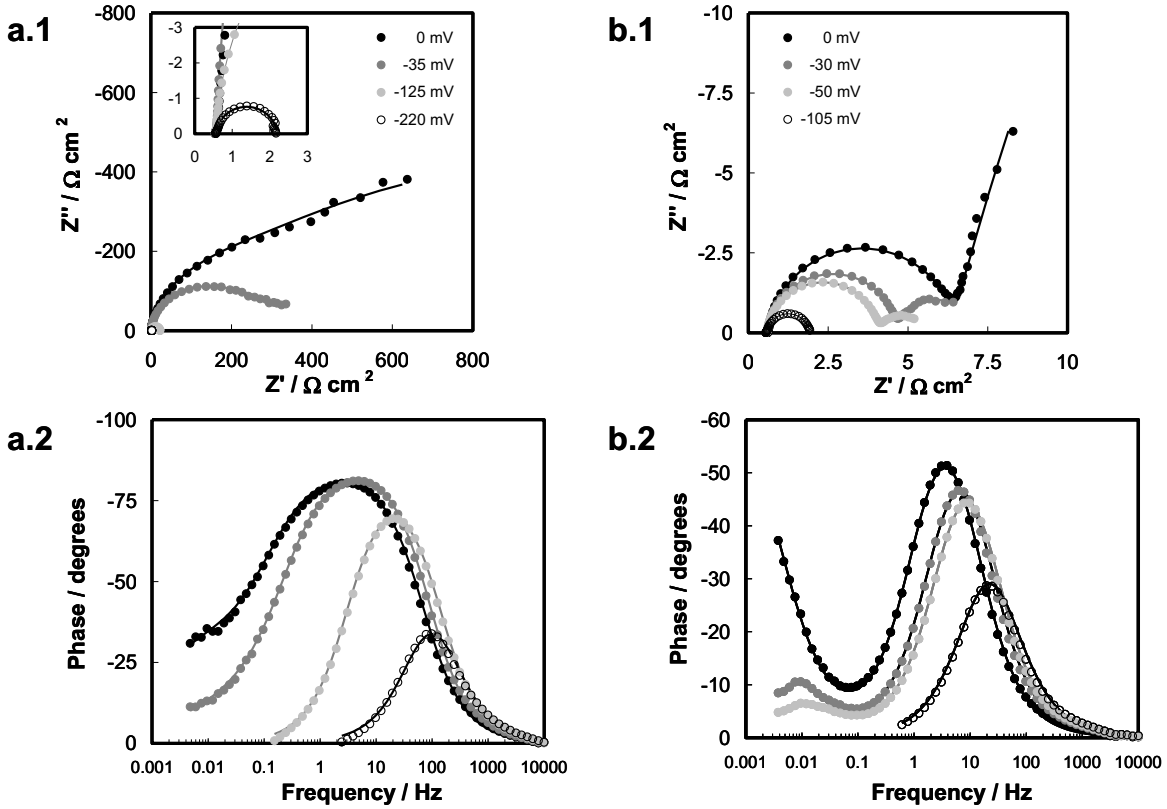

Figure 6. Impedance data obtained in 30 wt. % KOH solution at 30 ºC for: **a.** ED-2 catalyst: **a.1** Nyquist representation, **a.2** Bode representation of the phase angle as a function of frequency; and **b**. ED-4 catalyst: **b.1** Nyquist representation, **b.2** Bode representation of the phase angle as a function of frequency. Symbols are the experimental points and solid lines are modelled data.

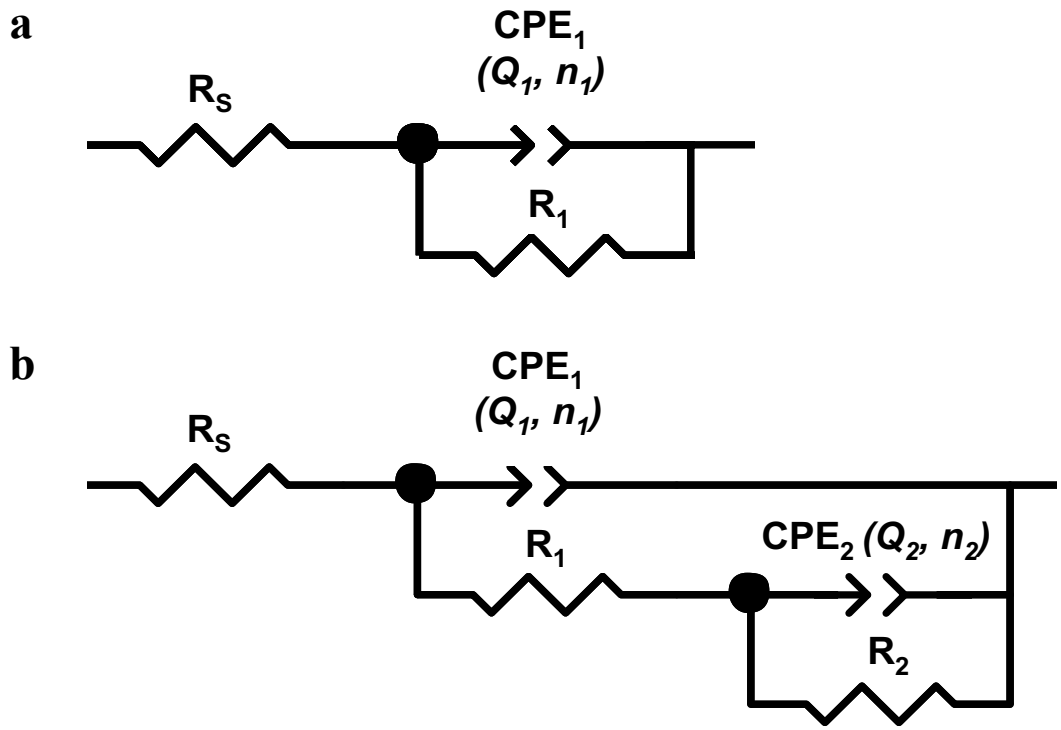

Figure 7. EEC models used to explain the EIS response of the HER on the developed electrocatalysts: **a**. one-time constant (1T), and **b**. two-time constant parallel model (2TP).

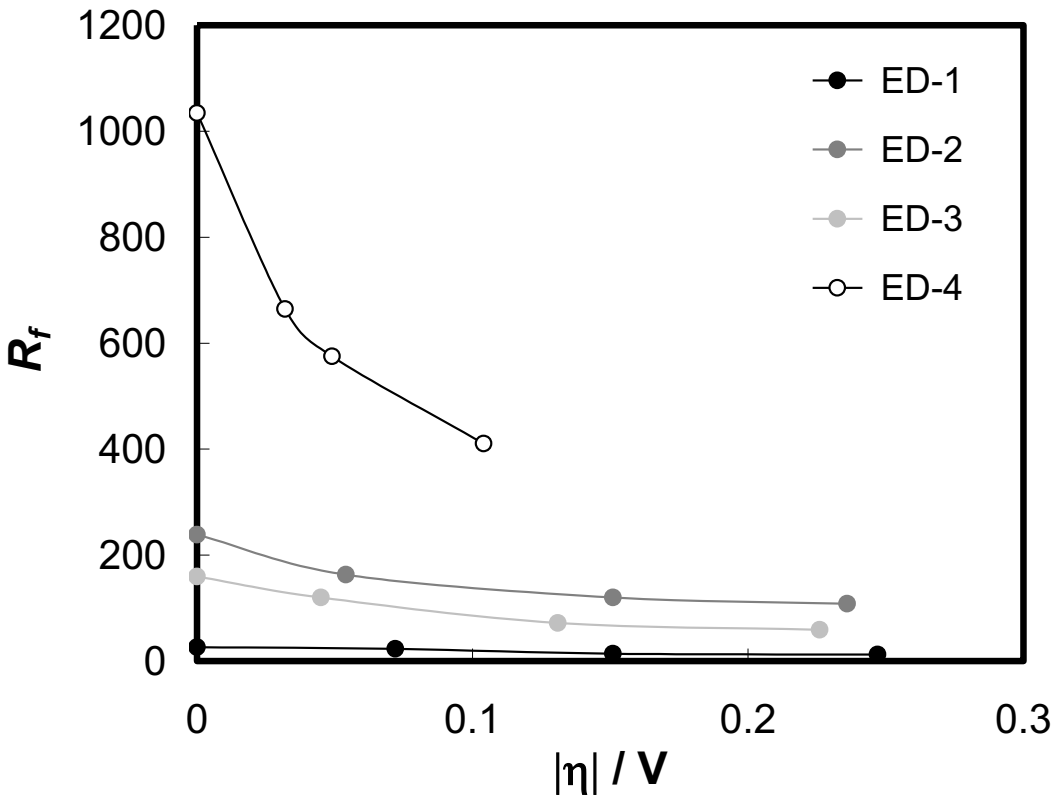

Figure 8. Surface roughness factor, R_f, as a function of the overpotential for the developed electrodes in 30 % wt. KOH solution at 50 ºC.